JJEE
Volume 11 | Number 1 | March 2025 | Pages 100-111

Jordan Journal of Electrical Engineering

ISSN (print): 2409-9600, ISSN (online): 2409-9619

Homepage: jjee.ttu.edu.jo

Experimental Evaluation of a Proposed LQR-LU Optimal Grid Controller in the Applications of Grid-Tied PV Systems

Angel Babita Muppidi[1], Hari Charan Nannam[2*]

[1, 2] Department of Electrical and Electronics Engineering, Vel Tech Rangarajan Dr. Sagunthala R&D Institute of Science and Technology, Chennai, Tamilnadu, India.
E-mail: drharicharan@veltech.edu.in

Received: May 16, 2024 *Revised: Aug 18, 2024* *Accepted: Aug 29, 2024* *Available online: Oct 1, 2024*

***Abstract*—** This article aims to design a linear quadratic regulator (LQR)-based optimal current controller along with a Luenberger observer model in order to enhance power quality during the grid's dynamic conditions. To analyze the performance of the proposed control scheme, a three-phase photovoltaic-based gird-tied inverter is considered. A grid controller comprises a DC-link voltage controller to stabilize the capacitor voltage and a current controller to assure the output currents are well controlled according to the dynamic conditions of the grid as well as the source. In general, the capacitor-voltage and current controllers are regulated by traditional proportional Integral (PI) controllers which is associated with many demerits. In this work, a predictive LQR-based current controller with an observer algorithm and an adaptive capacitor voltage controller is proposed to improve the performance of the power grid at various dynamic conditions. The mathematical analogy is evaluated using MATLAB/SIMULINK software with different load and grid-disturbance conditions. Moreover, a laboratory prototype is designed to validate the simulation results. The outcomes prove that the proposed controller is dynamically robust to tackle any disturbance in load and grid.

***Keywords*—** Voltage source inverter; Current controller; Grid-tied inverter; Linear quadratic regulator; Grid-tied PV system.

1. INTRODUCTION

A grid-tied photovoltaic generating station is the cleanest energy resource among all available non-conventional energy systems. Also, the photovoltaic system has a high modularity index, which means that even though larger power-rating plants are manufactured they can also be used for low-rated systems as well. It facilitates applications in a wider range, especially in residential smaller-scale roof-top areas to larger generations of power at the utility level [1]. The latest trends prove that power generation through renewable energy sources will rise continually in the upcoming years due to a reduction in the cost of their generation compared to their alternatives. The main merits of the non-conventional sources are their zero-emission of the CO_2 gases and a good alternative for fossil fuels. The higher investment cost and uncertainty of the source can be considered as the demerits of the system [2]. In the scenario of high-power production using renewable energy sources requires control due to their intermittent and destructive nature. So, a power converter interfacing is essential to control both the source and load constraints [3]. For the past thirty years, the power electronics industry has been changing rapidly due to the technological achievements in both semiconductor and control technologies. Also, the decrease in the cost of production has come down which increased their application in many areas of industrial and domestic arenas.

* Corresponding author
DOI: https://doi.org/10.5455/jjee.204-1715856762

The power electronic converters and the controller are intermediatory parts in the grid-tied renewable system as shown in Fig. 1. The power converter employed in the system should possess lesser losses and should be reliable and must work at higher switching values. A plethora of research work is available regarding power converters, their pulse width modulation (PWM) schemes, and applications [4]. The most commonly used power electronic converters are dc-dc converters and an inverter in traditional two-stage systems. Commonly the dc-dc converter works in step-up mode and tracks the maximum power from the available PV source. A review of dc-dc converters employed in renewable energy is presented in the literature [5]. Mostly voltage source inverters (VSI) are employed in the grid-tied renewable energy system. Among the VSIs, two-level and three-level (diode-clamped, flying capacitor, and cascaded-Bridge) inverters are commonly used as grid-tied inverters. The performance of the grid-integrated renewable energy system depends on the schemes of control employed for grid-tied inverters. It is explicitly known that the efficiency of renewable energy systems is low, and it can be further reduced if the control scheme employed can't provide optimum performance. If the parameters of the grid-tied renewable systems are not robustly controlled, it may lead to issues of stability and even may lead to failure [6]. To have a continuous and reliable power supply, the algorithms for synchronization and the grid side controllers play a vital role. In this regard, there was a huge exploration of the control schemes. An overview of all control schemes used for the grid-tied renewable energy systems is presented in [6]. Majorly the control schemes comprise (i) source control and (ii) grid control. A source controller's primary task is to track the peak power from the renewable source. It also enhances the input voltage, where the grid control has many parameters to control. It must control the active and reactive powers between the renewable source and the grid, the capacitor voltage control at the dc link, and currents injected into the grid with lower distortion and synchronization aspect of the grid. The grid control scheme comprises two loops which are cascaded. They are the capacitor voltage control loop which is an external one that regulates the voltage across the dc-link capacitor, as well as balances the flow of power from the source to the grid and the other is the current control loop which is an internal one and it controls the current injected into the grid with lower harmonic content and also responsible of protecting the system from grid related issues [7-12].

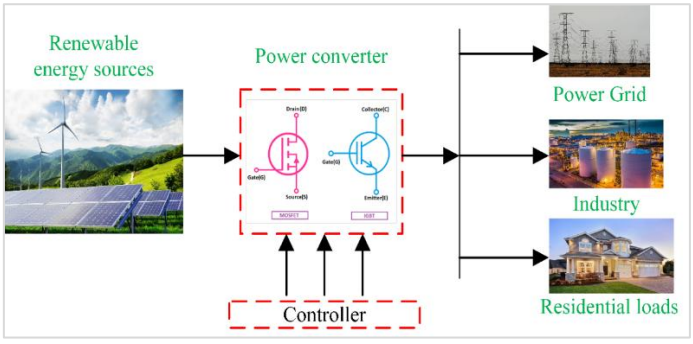

Fig. 1. The conventional block diagram of a controlled power converter-based renewable energy system.

The different control schemes used in the grid control are also presented in literature [13]. Among different controllers, model predictive controller (MPC) [14] is being extensively used in the areas of grid-tied renewable energy systems. In this work, the mathematical modeling of the grid-tied system is presented in Section 2, and the methodology of implementing the LQR-LU-based controller is presented in Section 3. The result analysis is presented in section 4 and finally, section 5 consists of a conclusion.

2. MATHEMATICAL MODELING OF THE PV-BASED GRID-TIED INVERTER SYSTEM

The complete block diagram of the system implemented is presented in Fig. 2. It consists of a photovoltaic system followed by a dc-dc converter to track the maximum power and enhance the voltage level. The terminal voltage of the dc-dc converter preferably the boost converter, is connected to the dc-link capacitor which serves as an input to the voltage source inverter (VSI). The VSI output is connected to the filter and is integrated into a power grid. The grid side control is controlled by an LQR-LU control scheme which will be elaborated in the following section. This section is dedicated to analyzing the mathematical modeling of the entire system.

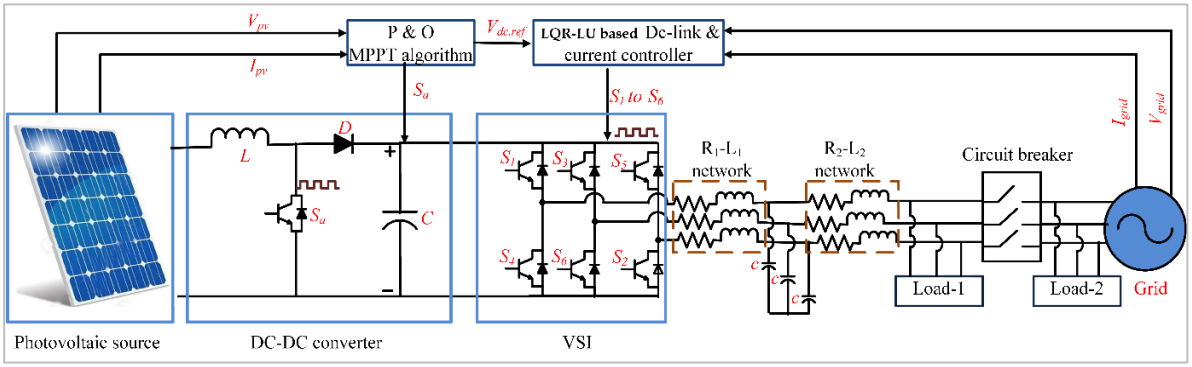

Fig. 2. The complete block diagram for a LQR-LU based controller for PV-based grid-tied renewable energy system.

2.1. Mathematical Modelling of the DC-DC Converter

The mathematical modeling of the photovoltaic system is elucidated in the literature [15]. The circuit diagram for the dc-dc converter is presented in Fig. 2. On considering the continuous conduction mode, the current increasing linearly from I_a to I_b takes T_1 time and the linear decrease (from I_b to I_a) takes T_2 time, then

$$T_1 = \frac{L*\Delta I}{V_{PV}} \quad (1)$$

$$T_2 = \frac{L*\Delta I}{V_C - V_{PV}} \quad (2)$$

where L is the inductor voltage, ΔI is the change in current from I_a to I_b, V_C is the voltage across the dc-link capacitor. The difference in the currents (ΔI) can be considered as the ripple quantity of the inductor current.

To achieve the average output voltage, substitute $T_1 = KT, T_2 = T - KT = (1-K)T$, then

$$V_C = V_{PV} * \frac{T}{T_2} = \frac{V_{PV}}{1-K} \quad (3)$$

On rearranging, the period of switching pulses can be derived as:

$$T = T_1 + T_2 = \frac{V_C * L * \Delta I}{V_{PV}(V_C - V_{PV})} \quad (4)$$

3. The Proposed LQR-LU Optimal Grid Controller

The dc-ac converter is considered to be connected to the grid through an LCL filter. A space vector pulse width modulation is implemented through the proposed controller to generate the triggering pulses to the converter. The control scheme comprises an LQR-based state observer and a controller based on the state-feedback concept while measuring only two

parameters of the grid (voltage and current). The block diagram for the grid-connected dc-ac system is presented in Fig. 3.

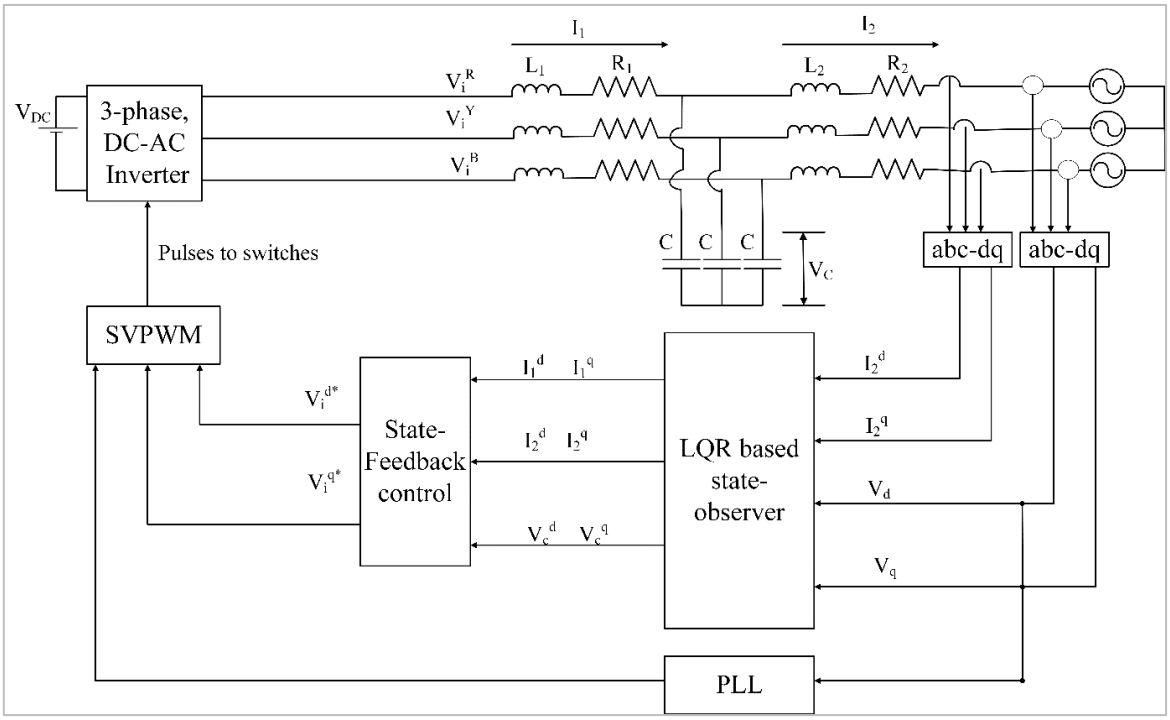

Fig. 3. Block diagram representation for the grid-tied converter system using LQR-state feedback control.

Using the synchronous frame of control and Park's transformation, the grid-tied inverter system can be modeled as [16]:

$$\begin{bmatrix} f_d \\ f_q \\ f_0 \end{bmatrix} = \frac{2}{3}\begin{bmatrix} cos\theta & \cos(\theta - \frac{2\pi}{3}) & \cos(\theta + \frac{2\pi}{3}) \\ sin\theta & \sin(\theta - \frac{2\pi}{3}) & \sin(\theta + \frac{2\pi}{3}) \\ \frac{1}{2} & \frac{1}{2} & \frac{1}{2} \end{bmatrix}\begin{bmatrix} f_a \\ f_b \\ f_c \end{bmatrix} \quad (5)$$

The variable "f" denotes the transformation variable and θ denotes the phase angle. The mathematical equations about inverter modeling are [16]:

$$i_{2,q} = -\left(\frac{R_2}{L_2}\right) i_{2,q} - \omega i_{2,d} + \left(\frac{1}{L_2}\right) * V_{C,q} - \frac{1}{L_2} * V_{g,q} \quad (6)$$

$$i_{2,d} = -\left(\frac{R_2}{L_2}\right) i_{2,d} + \omega i_{2,q} + \left(\frac{1}{L_2}\right) * V_{C,d} - \frac{1}{L_2} * V_{g,d} \quad (7)$$

$$i_{1,q} = -\left(\frac{R_1}{L_1}\right) i_{1,q} - \omega i_{1,d} - \left(\frac{1}{L_1}\right) * V_{C,q} + \frac{1}{L_1} * V_{i,q} \quad (8)$$

$$i_{1,d} = -\left(\frac{R_1}{L_1}\right) i_{1,d} + \omega i_{1,q} - \left(\frac{1}{L_1}\right) * V_{C,d} + \frac{1}{L_1} * V_{i,d} \quad (9)$$

$$V_{C,q} = -\omega V_{C,d} - \left(\frac{1}{C}\right) * i_{2,q} + \left(\frac{1}{C}\right) * i_{i,q} \quad (10)$$

$$V_{C,d} = -\omega V_{C,q} - \left(\frac{1}{C}\right) * i_{2,d} + \left(\frac{1}{C}\right) * i_{i,d} \quad (11)$$

where the grid frequency in radians per second is denoted by ω, i_1 denotes the currents flowing through the three-phase inverter, i_2 denotes the currents flowing into the grid, V_g denotes the grid voltage and V_i represents the inverter output voltage.

The mathematical representation of the VSI in the continuous-time domain is represented as:

$$\dot{X}(t) = A\,x(t) + Bu(t) + D.e(t) \quad (12)$$

$$Y(t) = C\mathrm{x(t)} \quad (13)$$

where $x(t) = \begin{bmatrix} i_{q,2} \\ i_{d,2} \\ i_{q,1} \\ i_{d,1} \\ V_{C,q} \\ V_{C,d} \end{bmatrix}$; $u\,(t) = \begin{bmatrix} V_{i,q} \\ V_{i,d} \end{bmatrix}$; $e(t) = \begin{bmatrix} e_q \\ e_d \end{bmatrix}$;

$$A = \begin{bmatrix} -R_2/L_2 & -\omega & 0 & 0 & 1/L_2 & 0 \\ \omega & -R_2/L_2 & 0 & 0 & 0 & 1/L_2 \\ 0 & 0 & -R_1/L_1 & -\omega & -1/L_1 & 0 \\ 0 & 0 & \omega & -R_1/L_1 & 0 & 1/L_1 \\ -1/C & 0 & 1/C & 0 & 0 & -\omega \\ 0 & -1/C & 0 & 1/C & \omega & 0 \end{bmatrix} \quad B = \begin{bmatrix} 0 & 0 \\ 0 & 0 \\ 1/L_1 & 0 \\ 0 & 1/L_1 \\ 0 & 0 \\ 0 & 0 \end{bmatrix}; \quad D = \begin{bmatrix} 0 & 0 \\ 0 & 1/L_2 \\ 1/L_1 & 0 \\ 0 & 0 \\ 0 & 0 \\ 0 & 0 \end{bmatrix}$$

$$C = \begin{bmatrix} 1 & 0 & 0 & 0 & 0 & 0 \\ 0 & 1 & 0 & 0 & 0 & 0 \end{bmatrix}$$

To implement the above system in digital mode, discrete modeling [17] is eminent with a discrete time of sampling T_s:

$$X(k+1) = A\,x(k) + B\,u(k) + D\,e(k) \tag{14}$$

$$Y(k) = C\,x(k) \tag{15}$$

where $A = 1 + \frac{AT_s}{1!} + \frac{A^2T^2}{2!} + \cdots;\ B = A^{-1}[A - I]B;\ D = A^{-1}[A - I]D$

The VSI is controlled by the Space vector pulse width scheme (SVPWM) as shown in Fig. 3. To enable the process of grid synchronization a phase-locked loop is utilized to detect the phase angle of the grid system. The terms related to integral and resonant in the state feedback controller are represented as [17]:

$$\begin{bmatrix} X_{i,q}(t) \\ X_{i,d}\,(t) \end{bmatrix} = \begin{bmatrix} 0 & 0 \\ 0 & 0 \end{bmatrix} \begin{bmatrix} x_{i,q}(t) \\ x_{i,d}\,(t) \end{bmatrix} + \begin{bmatrix} 1 & 0 \\ 0 & 1 \end{bmatrix} \begin{bmatrix} \epsilon_q(t) \\ \epsilon_d(t) \end{bmatrix} \tag{16}$$

$$\begin{bmatrix} \varepsilon_{1,i,q}(t) \\ \varepsilon_{2,i,q}(t) \\ \varepsilon_{1,i,d}(t) \\ \varepsilon_{2,i,d}(t) \end{bmatrix} = \begin{bmatrix} 0 & 1 & 0 & 0 \\ -\omega^2 & -2i\omega\xi & 0 & 0 \\ 0 & 0 & 0 & 1 \\ 0 & 0 & \omega^2 & -2i\omega\xi \end{bmatrix} \begin{bmatrix} \varepsilon_{1,i,q}(t) \\ \varepsilon_{2,i,q}(t) \\ \varepsilon_{1,i,d}(t) \\ \varepsilon_{2,i,d}(t) \end{bmatrix} + \begin{bmatrix} 0 & 0 \\ 1 & 0 \\ 0 & 0 \\ 0 & 1 \end{bmatrix} \begin{bmatrix} \epsilon_q(t) \\ \epsilon_d(t) \end{bmatrix} \tag{17}$$

where ξ denotes the damping coefficient.

4. RESULTS AND DISCUSSION

4.1. Simulation Analysis

In this work, the result analysis is carried out by using MATLAB/SIMULINK software. The effect of the solar irradiance on the dq components of the current is presented in Fig. 4. It is observed that the value of irradiance is changed at time t=0.05 and t=0.2. The reference values of the direct axis current set by the controller are 0.4A and 0.8A. Also, considering a unity power factor current, the current at the quadrature component is considered as zero. It is observed that the direct component of the current tracks the reference value accurately. Also, the quadrature component of the current is steadfastly concentrated at the zero value despite of sudden variation at the intermittent irradiance conditions. Similarly, the variations in the output voltage and currents at the inverter side after the filter are presented in Fig. 5. As the solar irradiance changes, the dc link voltage controller has to constantly monitor the dc-link voltage. The robust dc-link voltage controller has made the voltage across the capacitor constant which is evident from the voltage of the inverter after the filter terminals. The inverter output voltage has remained constant due to the constant voltage across the dc-link

capacitor irrespective of the change in solar irradiance. The impact of the dynamics is concentrated on the variable current quantity, as a result the current magnitude has increased at an increase in the solar irradiance.

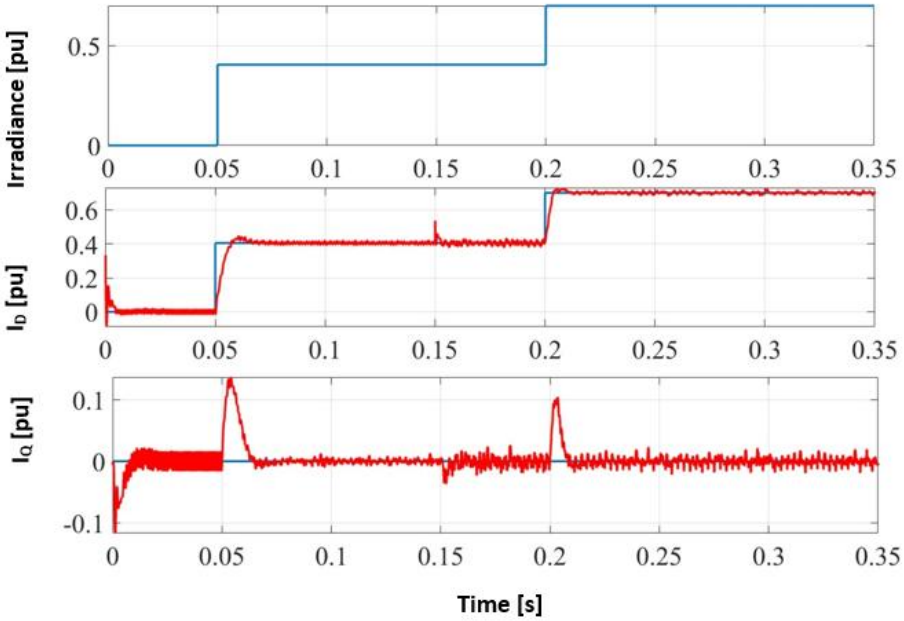

Fig. 4. Effect of the solar irradiance on the dq current components.

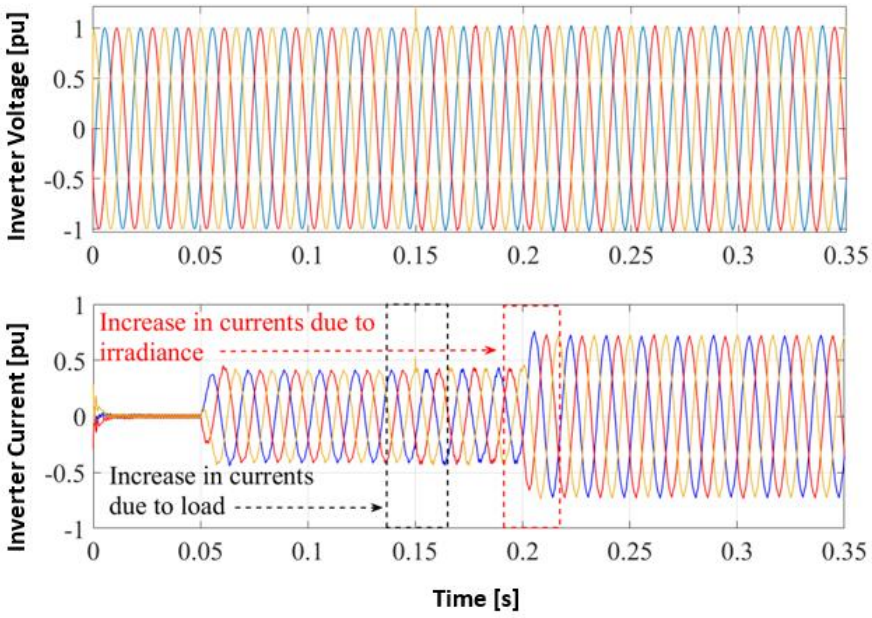

Fig. 5. Output voltage and current at the inverter side after the filter.

The analysis of active and reactive power is presented in Fig. 6. It is, that the reactive power component is maintained at zero to provide a unity power factor condition. The increase in solar irradiance has increased the power output from 0.5 p.u to 0.95 p.u., which is evident from Fig. 6. The analysis of the grid voltage and currents are presented in Fig. 7. The grid voltage is maintained constant, and the grid currents are in variable condition due to the proposed controller connected to the grid side. The grid supplies power to the load at the instant that the source is not able to deliver the necessary power due to low solar irradiance. The analysis of grid active and reactive powers is presented in Fig. 8. The rating of one of the

loads after the LCL filter is 50 kW and the other is 75 KW and a circuit breaker is connected between the two for creating a dynamic load analysis.

a) At time t=0.05s, the irradiance is increased, and it remains constant till t=0.2s. At t=2s, the irradiance is increased, and it remains constant until the end of simulation time.
b) A command is given to the circuit breaker to get disconnected from the grid till time t=0.1s. Once the simulation time crosses the instant t=0.15s, the circuit breaker connects the load-2 to the PV system.
c) Before the CB connects the load-2, the PV system feeds the power to load-1 and the grid feeds the power to load-2.
d) Due to the sudden connectivity of the load-2 at time t=0.15, the inverter must meet the both loads load-1 and load-2. It falls short of meeting the increase in load demand. As a result, the figure presented for inverter active and reactive power experiences a decrease in magnitude. At this instant, the grid supports the increase in load demand, as a result, the graph mentioned for grid active and reactive powers, the magnitude of the active power is increased.

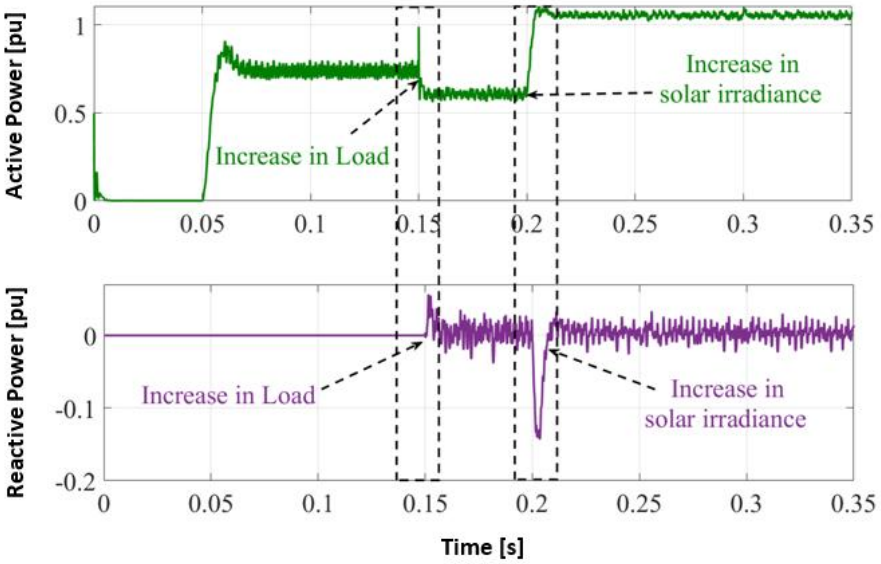

Fig. 6. Active and reactive powers at various load and solar irradiance conditions.

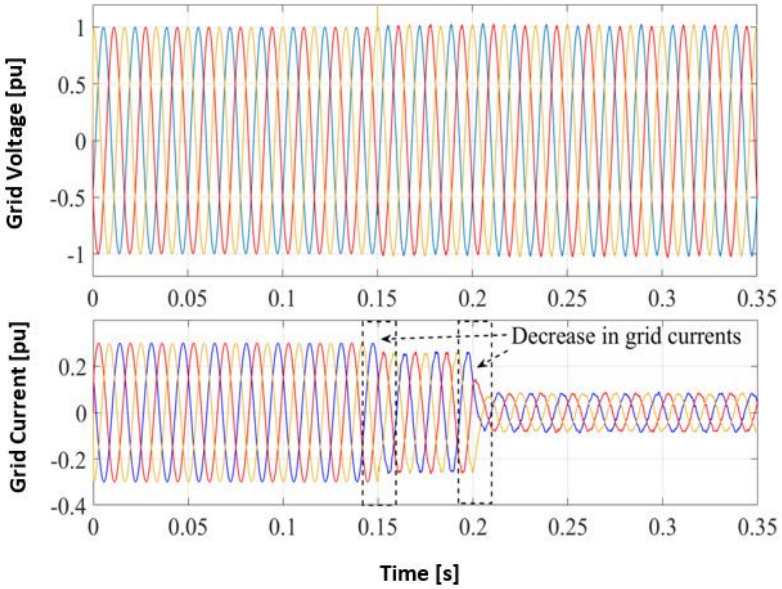

Fig. 7. Grid voltage and current at different load and irradiance conditions.

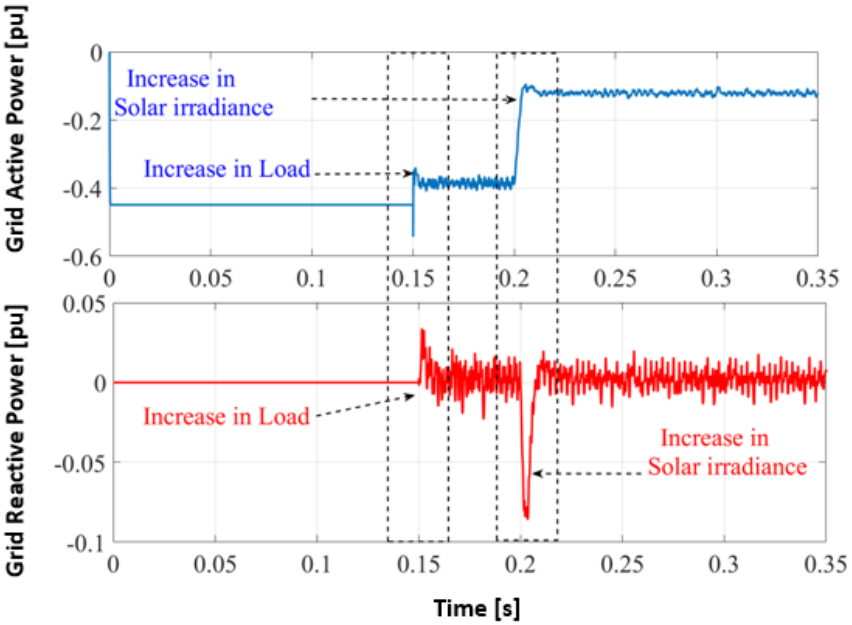

Fig. 8. Grid active and reactive powers.

4.2. Experimental Analysis

The experimental analysis for the proposed control scheme is presented in Fig. 9. The experimental prototype consists of a 1KW PV system with an SP-110 pyranometer to sense the solar irradiance. The solar irradiation is collected from the SP110 pyranometer. The analog sensor SP-110 is self-powered and has an output range of 0 to 400 mV. With a sturdy, self-cleaning sensor housing and a silicon-cell photodiode, the sensor includes a premium wire that ends in pre-tinned pigtail leads for a simple connection to dataloggers and controllers. An IP68 marine-grade stainless steel cable connector, located 30 centimeters from the sensor's head, makes removing and replacing the sensor for maintenance and calibration easier.

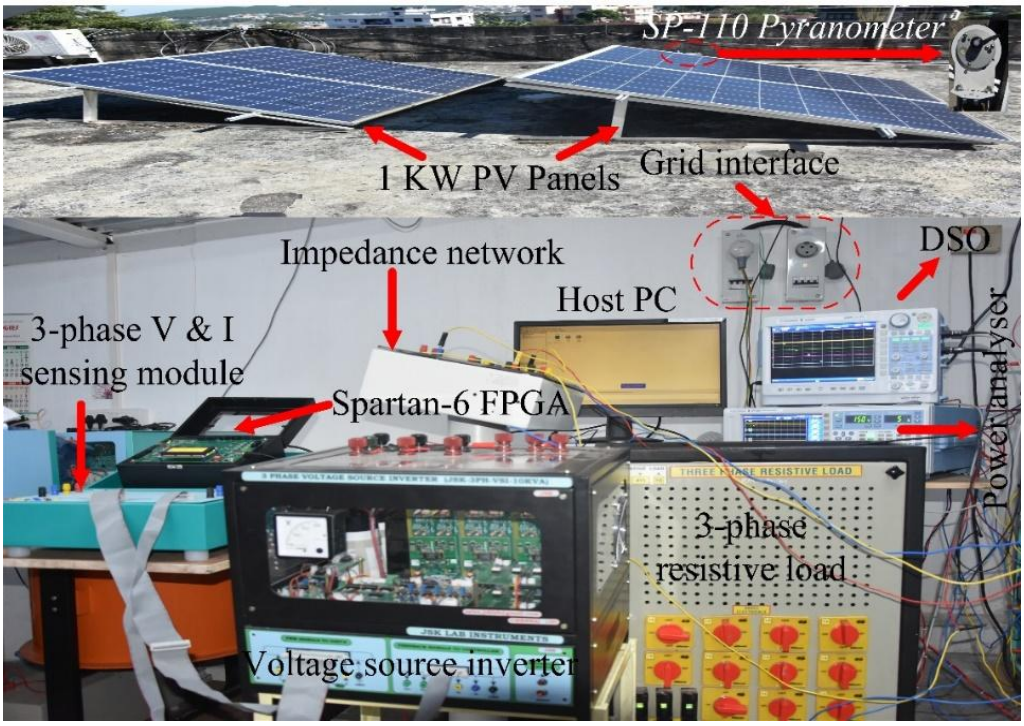

Fig. 9. The experimental prototype used to analyze the system.

The output of the SP-110 is in the voltage form, so Fig. 10 represents 200mV/division. According to the change in solar irradiance, the PV voltage and current vary as shown in Fig. 10. The PV voltage varies as 100V/division and the current varies as 5A/division. By using mathematical relations in DSO, the power is generated by multiplying the signal of PV voltage and current, that is represented as PV power which is calibrated at 500W/division. The voltage and current of the PV panel are connected to a dc-dc converter and a voltage source inverter module of 5KW as shown in Fig. 9.

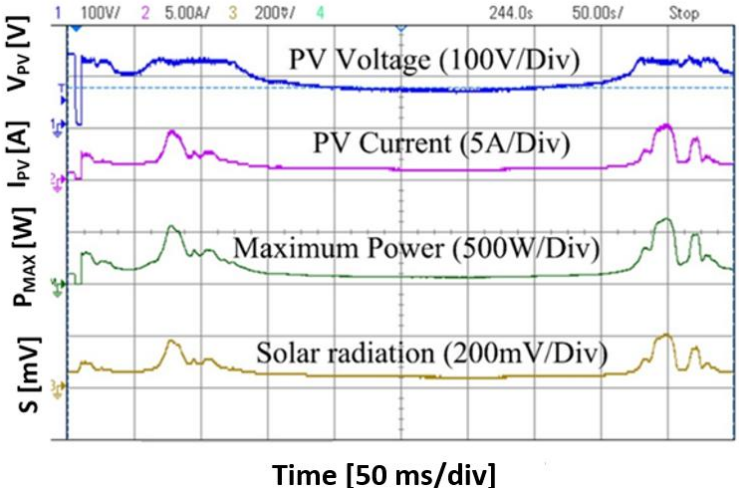

Fig. 10. PV voltage and current at different solar radiation conditions.

The FPGA spartan-6 board is used to implement the control algorithm that in turn generates the pulse pattern to the switches. Three-phase voltage and current sensing modules are presented on the grid side to feedback on the signals to the controller to formulate the proposed algorithm. A three-phase voltage and current sensors are used to sense the inverter output voltages and synchronize with the grid. Also, a three-phase load is connected at the inverter terminals to explore the dynamic nature of the load and its performance on the control system.

A Yokogawa power analyzer is used to evaluate the experiment output from the system, where a DSO is used to record the results of the PV system. The power analyzer is also used to find the THD content present in the grid's current. The analysis of PV voltage and current in a real-time environment is presented in Fig.10. The solar radiation and its change are presented in Fig.10. According to the change in solar radiation, the voltage and currents of the PV panels are changing. The maximum power output calibrated using an MPPT algorithm is calculated and presented in Fig. 10.

The analysis of load change and grid disturbance conditions are analyzed in Fig. 11 and Fig. 12, respectively. In Fig. 11, the load is suddenly increased and decreased at different time instants, but the LQR-based control scheme has generated the current which is by the reference. Similarly, the voltage sag and swell conditions of the system are perfectly analyzed by using the controller.

It was proved that the controller is dynamically robust enough to tackle any disturbance in load and grid. The analysis of the grid voltage and current is presented in Fig. 12.

The THD analysis of the proposed system is presented in Fig. 13. It is observed that the THD is 2.993% which is less than the IEEE standard. Also, the power factor is very near to unity. The amount of THD present in every voltage is presented in the analysis.

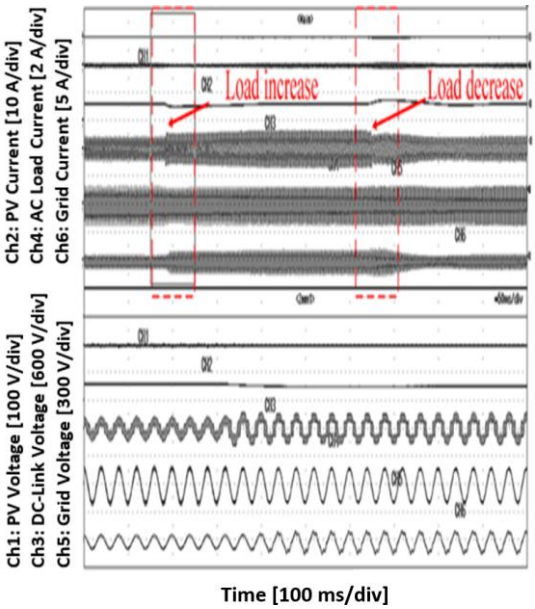

Fig. 11. Analysis of load variation effect on the proposed system.

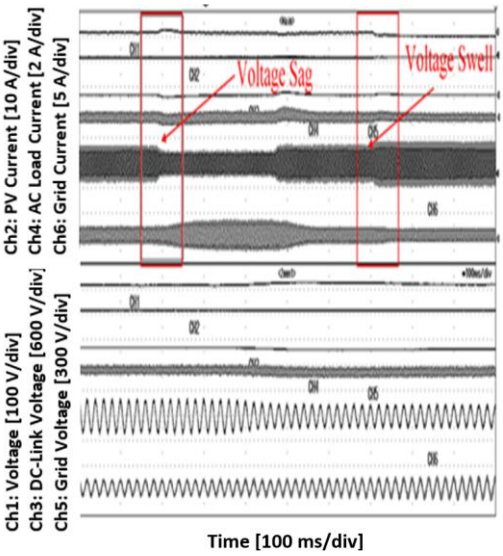

Fig. 12. The grid disturbance analysis using the proposed control scheme.

			Order	I1 [A]	hdf[%]	Order	I1 [A]	hdf[%]
fPLL1:U1	49.866	Hz	Total	2.8142		dc	---------	-------
			41	0.0049	0.174	42	0.0076	0.269
			43	0.0033	0.118	44	0.0050	0.178
Urms1	109.32	V	45	0.0012	0.044	46	0.0032	0.112
Irms1	2.8162	A	47	0.0017	0.061	48	0.0092	0.327
P1	306.24	W	49	0.0037	0.133	50	0.0045	0.161
S1	307.86	VA	51	0.0036	0.128	52	0.0037	0.131
Q1	-31.50	var	53	0.0029	0.101	54	0.0088	0.312
λ1	0.9948		55	0.0043	0.153	56	0.0078	0.278
Φ1	D5.87	°	57	0.0041	0.146	58	0.0064	0.229
			59	0.0064	0.226	60	0.0039	0.138
Uthd1	2.763	%	61	0.0046	0.164	62	0.0027	0.096
Ithd1	2.933	%	63	0.0059	0.211	64	0.0023	0.080
Pthd1	0.004	%	65	0.0061	0.218	66	0.0034	0.120
Uthf1	1.561	%	67	0.0058	0.207	68	0.0052	0.186
Ithf1	2.520	%	69	0.0039	0.139	70	0.0068	0.241
Utif1	67.240		71	0.0025	0.088	72	0.0028	0.099
Itif1	116.282		73	0.0067	0.240	74	0.0050	0.177
hvf1	1.009	%	75	0.0042	0.149	76	0.0072	0.258
hcf1	1.086	%	77	0.0030	0.107	78	0.0075	0.267
Kfact1	1.8392		79	0.0036	0.130	80	0.0047	0.168
PAGE 1/8						PAGE 2/13		

Fig. 13. THD analysis of the grid voltage and current.

5. CONCLUSIONS

In this work, the detailed explanation of the mathematical modeling of a two-stage system is elucidated in detail. The analysis of the proposed LQR-based control scheme is well analyzed with mathematical equations. The simulation and experimental analysis were carried out to find the optimal performance of the system at different dynamic conditions. The load analysis and grid disturbance conditions were chosen to mitigate them by using the proposed controller. The outcomes prove the robustness of the controller. The system performance can be precisely improved using model predictive control methods which will be focused on further. The limitations of the proposed controller are:

- The assumption that the system is devoid of outside disturbance and measurement noise is a third drawback of LQR. These elements, however, unavoidable in real systems, have the potential to deteriorate both the quality of the control and the tracking performance. Disturbance rejection techniques, including feedforward control, integral action, or Kalman filter, can be used to estimate and correct noise and disturbance to address this issue.
- The inability of LQR to take into consideration the controller's and system's physical limitations is a fourth limitation. Constrained LQR (CLQR), which integrates the constraints into the optimization problem, can be used to overcome this issue
- The last issue with LQR is that it can be difficult to apply and computationally difficult, particularly for large-scale, high-dimensional, or nonlinear systems. The matrix Riccati equation for the LQR controller must be solved, which can be laborious and numerically unstable.

Acknowledgment: The authors would like to thank the management and R&D office staff of VelTech Rangarajan Dr. Sagunthala R&D Institute of Science and Technology for the constant support in providing the SEED fund with reference no. VTU SEED (FY 22-23)-19 to design the laboratory prototype and to carry out this research work.

REFERENCES

[1] M. Kandil, M. Aly, M. Akl, M. Iqbal, "Monitoring system for a hybrid photovoltaic-diesel power system: web-based SCADA approach," *Jordan Journal of Electrical Engineering*, vol. 9, no. 1, pp. 1-13, 2023, doi**:** 10.5455/jjee.204-1669826483

[2] M. Ahmed, S. Mirsaeidi, M. Koondhar, N. Karami, E. Tag-Eldin, N. Ghamry, R. El-Sehiemy, Z. Alaas, I. Mahariq, A. Sharaf, "Mitigating uncertainty problems of renewable energy resources through efficient integration of hybrid solar PV/wind systems into power networks," *IEEE Access*, vol. 12, pp. 30311-30328, 2024, doi: 10.1109/ACCESS.2024.3370163

[3] T. Mir, B. Singh, A. Bhat, "FS-MPC-Based speed sensorless control of matrix converter fed induction motor drive with zero common mode voltage," *IEEE Transactions on Industrial Electronics*, vol. 68, no. 10, pp. 9185-9195, 2021, doi: 10.1109/TIE.2020.3020031

[4] F. Blaabjerg, Y. Yang, K. Kim, J. Rodriguez, "Power electronics technology for large-scale renewable energy generation," *Proceedings of the IEEE*, vol. 111, no. 4, pp. 335-355, 2023, doi: 10.1109/JPROC.2023.3253165.

[5] W. He, Y. Zhang, W. Zhou, "Observerless output feedback control of DC-DC converters feeding a class of unknown nonlinear loads via power shaping," *IEEE Transactions on Circuits and Systems I: Regular Papers*, vol. 71, no. 6, pp. 2951-2963, 2024, doi: 10.1109/TCSI.2024.3369242.

[6] Q. Liu, T. Caldognetto, S. Buso, "Review and comparison of grid-tied inverter controllers in microgrids," *IEEE Transactions on Power Electronics*, vol. 35, no. 7, pp. 7624-7639, 2020, doi: 10.1109/TPEL.2019.2957975.

[7] H. Nannam, A. Banerjee, J. Guerrero, ''Analysis of an interleaved control scheme employed in split source inverter based grid-tied photovoltaic systems,'' *IET Renewable Power Generation*, vol. 15, no 6. pp. 1301–1314, 2021, doi: 10.1049/rpg2.12108

[8] H. Zamani, K. Abbaszadeh, M. Karimi, J. Gyselinck, "Adaptive model predictive control for LCL-filter grid-tied inverters," *IEEE Transactions on Industrial Electronics*, vol. 71, no. 8, pp. 8903-8914, 2024, doi: 10.1109/TIE.2023.3325574.

[9] S. Nam, J. Kim, Y. Kim, O. Bellmunt, "Adaptive-observer-based control of a real-world grid-forming converter-interfaced shaft generator in a shipboard microgrid," *IEEE Transactions on Industrial Electronics*, vol. 71, no. 9, pp. 11429-11440, 2024, doi: 10.1109/TIE.2023.3335468

[10] W. Xiao, G. Jiang, J. Mao, F. Xie,B. Zhang, D. Qiu, Y. Chen, "Adaptive logarithmic state feedback control with quasi one-switching-cycle response characteristic for three-phase inverter," *IEEE Transactions on Circuits and Systems II: Express Briefs*, vol. 71, no. 6, pp. 3046-3050, 2024, doi: 10.1109/TCSII.2024.3353491.

[11] D. Pal, B. Panigrahi, "Impact of DC-bus voltage control on synchronization stability of grid-tied inverters," *IEEE Transactions on Circuits and Systems II: Express Briefs*, vol. 69, no. 6, pp. 2782-2786, 2022, doi: 10.1109/TCSII.2022.3152273.

[12] S. Swain, B. Subudhi, "Grid synchronization of a PV system with power quality disturbances using unscented kalman filtering," *IEEE Transactions on Sustainable Energy*, vol. 10, no. 3, pp. 1240-1247, 2019, doi: 10.1109/TSTE.2018.2864822

[13] S. Ahmad, M. Shafiullah, C. Ahmed, M. Alowaifeer, "A review of microgrid energy management and control strategies," *IEEE Access*, vol. 11, pp. 21729-21757, 2023, doi: 10.1109/ACCESS.2023.3248511

[14] X. Wang, J. Hu, C. Garcia, J. Rodriguez, B. Long, "Robust sequential model-free predictive control of a three-level T-type shunt active power filter," *IEEE Transactions on Power Electronics*, vol. 39, no. 8, pp. 9505-9517, 2024, doi: 10.1109/TPEL.2024.3403831.

[15] X. Geng, B. Zhang, D. Qiu, Y. Chen, W. Xiao, F. Xie, "Modeling and nonlinear dynamic analysis of a photovoltaic system with multiple parallel branches based on simplified discrete time model," *IEEE Transactions on Power Electronics*, vol. 39, no. 8, pp. 10226-10238, 2024, doi: 10.1109/TPEL.2024.3388577

[16] J. Montenegro, F. Andrade, J. Guerrero, J. Vasquez, "A linear quadratic regulator with optimal reference tracking for three-phase inverter-based islanded microgrids," *IEEE Transactions on Power Electronics*, vol. 36, no. 6, pp. 7112-7122, 2021, doi: : 10.1109/TPEL.2020.3036594.

[17] S. Gao, D. Zhao, X. Yan, S. K. Spurgeon, "Model-free adaptive state feedback control for a class of nonlinear systems," *IEEE Transactions on Automation Science and Engineering*, vol. 21, no. 2, pp. 1824-1836, 2024, doi: 10.1109/TASE.2023.3237811.